Transmission Nuclear Resonance Fluorescence Measurements of ^{238}U in Thick Targets

B.J. Quiter[a,b,*], B.A. Ludewigt[b], V.V. Mozin[a,c], C. Wilson[d], S. Korbly[d]

[a] *Department of Nuclear Engineering, University of California, Berkeley, CA*
[b] *Lawrence Berkeley National Laboratory, Berkeley, CA*
[c] *Los Alamos National Laboratory, Los Alamos, NM*
[d] *Passport Systems, Incorporated, Bilerica, MA*

Abstract

Transmission nuclear resonance fluorescence measurements were made on targets consisting of Pb and depleted U with total areal densities near 86 g/cm^2. The ^{238}U content in the targets varied from 0 to 8.5% (atom fraction). The experiment demonstrates the capability of using transmission measurements as a non-destructive technique to identify and quantify the presence of an isotope in samples with thicknesses comparable to the average thickness of a nuclear fuel assembly. The experimental data also appear to demonstrate the process of notch refilling with a predictable intensity. Comparison of measured spectra to previous backscatter ^{238}U measurements indicates general agreement in observed excited states. Evidence of two new ^{238}U excited states and possibly a third state have also been observed.

Keywords: nuclear resonance fluorescence, transmission, U-238, non-destructive assay, notch refill

1. Introduction

Nuclear resonance fluorescence (NRF) has been a known phenomenon for many years. The original interest was primarily devoted to nuclear structure studies[1], however the process has also been used for non-destructive isotopic measurements of ^{13}C for diamond formation studies[2], and more recently, has been identified as a potential technology for cargo screening[3, 4, 5, 6] and nuclear safeguards[6, 7, 8].

NRF signatures are most commonly measured by either a backscatter or a transmission measurement[9, 10]. In both measurement techniques, a source photon beam is used to induce nuclear excitations in a target. The rate at which NRF occurs in the target is proportional to the amount of the corresponding isotope contained therein. Hence, measurement of the amount of an isotope present in a target is accomplished by determining the rate at which the isotope undergoes NRF. In the backscatter method, this rate is determined by measuring the fluorescence γ-rays using radiation detectors positioned at backwards locations, relative to the beam incident upon the target. In a transmission measurement, the rate at which NRF occurs in the target is determined by the attenuation of resonant-energy photons, which causes a reduced NRF rate in a sheet of the same isotope located further along the beam trajectory. This sheet is herein referred to as the transmission detection sheet.

In this paper, we describe transmission NRF measurements of ^{238}U in thick targets using bremsstrahlung. The target dimensions were selected to have an areal density and attenuation properties similar to a nuclear fuel assembly so that the applicability of the transmission method as a non-destructive measurement technique to quantify minor actinide content in nuclear fuel could be tested. In this experiment, Pb was used as a surrogate for the UO_2 matrix in spent fuel and the ^{238}U in depleted uranium (DU), was used as a surrogate for ^{239}Pu or any other minor actinide that would be measured in spent fuel. The DU sheets were 99.799% ^{238}U by mass, and the remaining portion of the DU was mostly ^{235}U. The amount of ^{238}U used in the experiment represents significantly higher concentrations than those of minor actinides in spent fuel. These amounts were selected to demonstrate the transmission attenuation effect in a timely manner using readily available radiation detectors and photon sources. A similar measurement has been made using thinner targets and a quasi-monoenergetic photon source[4]. This measurement reported a null result for the observation of the notch refill phenomenon, whereas the data presented here indicate notch refill has occurred. The process of notch refill will be discussed in Section 3.

The transmission measurement also provided information regarding ^{238}U states that undergo NRF. γ-rays due to ^{238}U NRF that had previously been reported by Heil et al.[11] were again observed. Six additional γ-rays have also been observed. These data are presented in Section 7.

2. Nuclear Resonance Fluorescence Signatures

States that undergo NRF are described by the total width, Γ, which is the sum of partial widths for different de-excitation modes, $\Gamma = \sum \Gamma_i$. De-excitation to the ground state by emission of a γ-ray is described with a width, Γ_0, and likewise, de-excitation to the first-excited state, by Γ_1. The cross section for a photon of energy, E, to excite a nucleus to a resonance with

*bjquiter@lbl.gov

centroid energy, E_C, is given by the Breit-Wigner distribution.

$$\sigma_{\mathrm{NRF}}(E) = \pi g \frac{(\hbar c)^2}{E^2} \frac{\Gamma\Gamma_0}{(E - E_c)^2 + (\Gamma/2)^2} \quad (1)$$

Where, g is a statistical factor equal to the ratio of the number of spin states available for the excitation relative to the number of initial spin states. For NRF events initiating from nuclear ground states,

$$g = \frac{2J + 1}{2(2J_0 + 1)} \quad (2)$$

where J and J_0 are the total angular momentum quantum numbers of the excited and ground states, respectively, and the additional factor of two in the denominator is due to the helicity of the exciting photon.

Integration of Equation 1 over all energies $E \geq 0$ does not converge on account of the singularity at $E = 0$. However, $E = 0$ photons are non-physical, and for a small lower energy integration limit, ϵ, the integral converges. If $\Gamma \ll E_c$,

$$\begin{aligned} \int_\epsilon^\infty \sigma_{\mathrm{NRF}}(E)dE &\approx \int_0^\infty \pi g \frac{(\hbar c)^2}{E_c^2} \frac{\Gamma\Gamma_0}{(E - E_c)^2 + (\Gamma/2)^2} dE \\ &= 7684[\mathrm{b} \cdot \mathrm{MeV}^2] \frac{\Gamma_0}{E_C^2} g \end{aligned} \quad (3)$$

This implies that the total strength of a resonance is determined by Γ_0 and its centroid energy. However, the probability for a NRF event that results in de-excitation to the ground state by a single γ-ray emission is given by Γ_0/Γ. Therefore backscatter measurements are sensitive to quantities such as Γ_0^2/Γ or $\Gamma_0\Gamma_1/\Gamma$, but cannot directly measure Γ_0 or Γ, unless all de-excitation modes are observed. Conversely, transmission measurements are most sensitive to the integrated cross section, which dictates the rate of resonant-energy photon absorption.

Atoms are generally in thermal motion causing photons to experience a cross section distribution that is Doppler-broadened.

$$\sigma_D(E) = \frac{1}{\sqrt{2\pi}\Delta} \int_0^\infty dE' \sigma_{\mathrm{NRF}}(E') \exp\left[\frac{-(E' - E)^2}{2\Delta^2}\right] \quad (4)$$

Where we define the Doppler width, Δ, for an atom with mass, M, at an effective temperature, T[1], as

$$\Delta = E_c \sqrt{\frac{k_B T}{Mc^2}} \quad (5)$$

For emission of a 2.176 MeV γ-ray from a ^{238}U nucleus at an effective temperature $T = 312$ K, the Doppler-width, $\Delta = 0.754$ eV. This width is significantly larger than the natural width, Γ, of all resonances considered herein and therefore effectively describes the width of the resonance. However, Δ is also much smaller than the energy resolution of germanium detectors for detection of photons of these energies.

[1]Effective temperatures are generally slightly higher than the ambient temperature to take account of the binding energy of solid materials. Calculations of T are described in reference[9].

Heil et al. observed NRF in ^{238}U by measuring discrete γ-rays in the backscattered photon spectrum of a bremsstrahlung beam incident upon a ^{238}U target[11]. These observed states are listed in Table 1. However, it had been assumed that the total width of each resonance was given by $\Gamma = 1.05\,\Gamma_0 + \Gamma_1$, which was not assumed by the nuclear data evaluators[12]. The influence of this assumption is examined in the discussion surrounding Table 4.

Table 1: Previously observed ^{238}U NRF states. Values of Γ_0^2/Γ and Γ_1/Γ_0 were taken from Heil et al.[11] where γ-ray emission to the ground state and first-excited state of ^{238}U ($J^\pi = 2^+$) at 44.92 keV were measured. The final column is calculated from Equation 3 assuming $\Gamma = \Gamma_0 + \Gamma_1$.

E_{level} (MeV)	Γ_0^2/Γ (meV)	Γ_1/Γ_0	$\int \sigma dE$ (eV·b)
2.176	23.7 ± 1.4	0.52 ± 0.02	87.7
2.209	22.6 ± 1.4	0.55 ± 0.03	82.7
2.245	13.4 ± 0.9	0.47 ± 0.03	45.0
2.295	5.3 ± 0.5	0.59 ± 0.10	14.4
2.410	11.0 ± 0.7	0.54 ± 0.05	33.6
2.468	13.4 ± 1.0	0.50 ± 0.05	38.0

3. Notch Refill

The term *notch refill* is used to describe the process by which photons incident upon the assay geometry down-scatter to the energy of a resonance and subsequently interact in the transmission detection sheet. The process results in less observed resonant attenuation than would be predicted by consideration of simple exponential attenuation, and therefore neglect of the notch refill phenomenon results in NRF transmission measurements that systematically under-predict the areal density of the measured isotope in the target.

Photon interaction processes that can induce notch refill include incoherent scatter and bremsstrahlung emission from photoelectrons. The rate at which notch refill occurs is dependent upon the compositions of the assay target and transmission detection sheet, their respective positioning, the energy and strength of a resonance, and the photon spectrum used for the measurement.

Generally, notch refill cannot be directly measured because the energy resolution required for such a measurement is approximately 1 eV for a resonance at 2 MeV. However, the processes that result in notch refill are readily computed using Monte Carlo radiation transport computer codes such as MCNPX[13]. Comparing MCNPX calculations with models that exclude notch refill gives an estimate of the notch refill intensity. As discussed in Section 6, the intensity of the notch refill corrections appears to be consistent with the measured data.

This method for determining notch refill would induce no systematic error if the down-scattered spectrum of photons calculated by MCNPX accurately represented reality. The photon transport routines used in the MCNPX code are fairly straightforward and widely used, it is therefore the quality of the photon scatter data and the statistical uncertainty in the simulations

that limit the accuracy of the notch refill correction. The photoatomic data used in MCNPX are derived from the evaluated photon data library (EPDL97) which states that photon cross sections should be accurate with less than 1% uncertainty[14]. The statistical uncertainties of the simulations on which the notch refill estimation is made are likewise near 1%. However, the notch refill correction is applied to the difference between the attenuation of resonant-energy photons calculated by MCNPX and those predicted analytically. This results in non-negligable uncertainties in the intensity of the notch refill effect. Because of this, predicted rates of resonant attenuation are presented with and without notch refill in Table 4, and the effects of the uncertainty of the notch refill arediscussed in Section 8.

Transmission experiments have previously neglected notch refilling because target areal densities were generally significantly smaller than in this experiment[4, 9, 10]. Thinner target thicknesses are better for measurement of resonant state parameters, but the target thicknesses selected for this experiment were intended to be representative of nuclear fuel assemblies. These thicker targets cause notch refill to be no longer negligible, and the positioning of DU and Pb in the targets was further selected to maximize the notch refill effect by placement of the Pb, which induced scatter but no NRF, downstream of the resonantly absorbing DU.

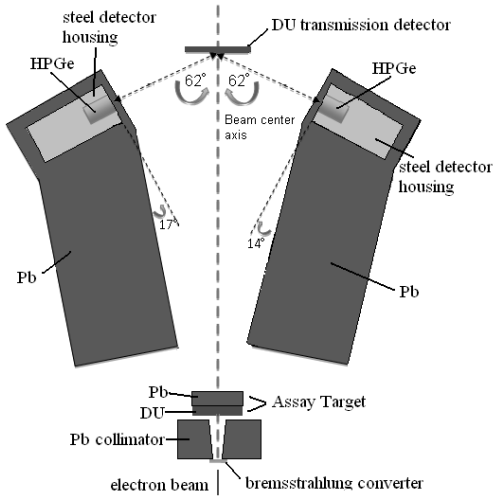

Figure 1: Schematic view of experimental setup. DU thicknesses have been exaggerated for visibility.

4. Experimental Setup

The experiment was conducted at the High Voltage Research Laboratory at Massachusetts Institute of Technology. Electrons accelerated to 2.60 ±0.03 MeV by a Van de Graaff accelerator are transported through a beamline, bent 90 degrees, and enter the bottom of the experimental geometry shown in Figure 1. They then impinge upon a converter target consisting of a 102 μm-thick Au layer on a 1 cm-thick water-cooled Cu backing. The electron current incident upon the converter was approximately 65 μA throughout the experiment. The bremsstrahlung emitted from the converter target is shaped by a 20 cm-thick Pb collimator. The diameter of the collimator opening was 1 cm on the bremsstrahlung converter side, and increased to 2.5 cm, resulting in a 3.6^{o} opening from the beam center, and a maximum angular acceptance of 5^{o}.

In Figure 1, there are five important features: the bremsstrahlung converter and collimator, the assay target, the transmission detection sheet, the high-purity Ge detectors and the Pb shielding. The assay target, a combination of DU and Pb, was located directly downstream of the collimator opening. The areal densities of DU and Pb used in the assay targets are summarized in Table 2. All targets were composed of metal sheets that were significantly larger than the diameter of the bremsstrahlung beam at the collimator outlet. This ensures the entirety of the beam penetrates the thickness of the target materials and reduces the sensitivity of the measurements to the positioning of the targets, relative to the beam. The DU was placed up-stream of the Pb in the beam, setting up the most probable geometry for notch refill.

The transmission detection sheet was placed 142 cm beyond the collimator opening and was not moved throughout the ex-

Table 2: Assay target compositions. Pb density assumed to be 11.34 g/cm^3, DU sheets were assumed to be 99.799% ^{238}U by mass. Uncertainties in DU masses are approximately 1%.

run	ρx_{DU} (g/cm^2)	ρx_{Pb} (g/cm^2)	total ρx (g/cm^2)	^{238}U atom%
1	0	86.26	86.26	0
2	8.47	79.85	87.86	8.48
3	1.69	85.20	86.80	1.69
4	3.34	83.37	86.54	3.37

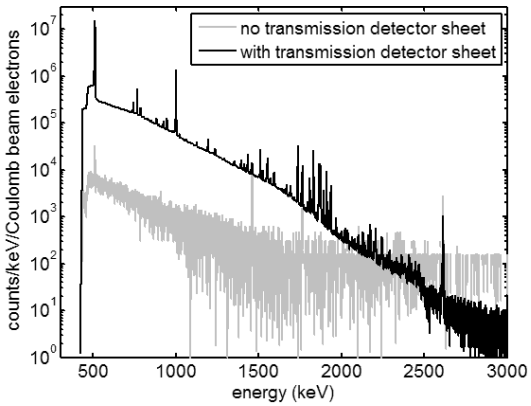

Figure 2: Measured spectra due to 2.6 MeV endpoint energy bremsstrahlung beam incident upon the run 1 target with and without the DU transmission detection sheet present downstream in the beam.

periment. It consisted of five 20.32 cm x 20.32 cm DU sheets that were nominally 0.8 mm-thick. Each sheet was contained in two plastic bags. The total mass of the five plates plus the containment bags was measured to be 3341.7 ± 3.3 g, of which 3226.7 ± 28 g are attributed to the DU. Behind the DU plates, 82.3 ± 0.5 g of Mn and 185.1 ± 0.8 g of 99.52% enriched ^{11}B were also positioned in the beam to serve as auxiliary flux monitors. Maintaining a fixed transmission detection sheet position between runs was critical to allow different measurements to be compared without incurring systematic errors due to changes in the transmission detection sheet positioning.

Two pairs of approximately 100% relative efficiency high-purity germanium detectors were positioned 27 cm from the intersection of the beam center and the transmission detection sheet, at an angle of 118^{o} relative to the centroid beam direction. Actual detector acceptances were distributed around the centroid angle with an approximate 10^{o} width. The detectors were contained in steel housings that were stacked in pairs, resulting in one detector being centered 4.5 cm above the beam center and the other centered 7 cm below the beam center.

Pb brick walls with minimum thicknesses of 80 cm were constructed to shield the radiation detectors from the bremsstrahlung converter and assay target. The detectors were also shielded with 5 cm of Pb in the down-stream direction, 10 cm of Pb below and behind the detectors, 17 cm of Pb above the detectors, and with a 1.27 cm-thick Pb *filter* facing the transmission detection sheet. The filter reduces the intensity of low-energy photons emitted from the transmission detection sheet due to Compton scatter and other processes.

To determine the contribution to measured spectra due to scatter of the bremsstrahlung beam in the assay target, a short measurement of the beam-on spectrum was conducted before the transmission detection sheet was positioned downstream of the assay target. A comparison of the gross detected spectra, before and after placement of the transmission detection sheet, are shown in Figure 2. Although the background run was significantly shorter, the two spectra were normalized by the integrated electron current that was measured with an ammeter to be deposited into the otherwise electrically isolated bremsstrahlung converter. The total count rate with the transmission detection sheet present increased by a factor of 100, and the rate at which 511 keV photons were detected increased by a factor of 500.

Each target was irradiated for approximately 7 hour measurements. The electron beam current was nominally 65 μA for each irradiation. The detectors were operated with Ortec DSPEC Pro^{TM} digital γ-ray spectrometers. The integrated pulse amplitudes were read and stored using MAESTRO-32 and a personal computer. In this configuration, the ADC rates were approximately 10^4 counts per second and the measured dead times were between 10 and 15% of livetime.

5. Data Analysis

Spectra were collected during four day-long irradiation shifts and background spectra, with no electron beam incident upon the bremsstrahlung converter, were collected overnight. The radioactivity of the DU and ambient ^{40}K provided lines for energy-calibrating the detectors. The γ-ray energies used for energy calibration are shown in Table 3. After calibrating the four detectors, their spectra were re-binned to a common energy grid and summed to provide a single spectrum for each target. An example of spectral summing is provided in Figure 3. After summing, peaks that were present in spectra taken during irradiations but not in background spectra were attributed to NRF.

Table 3: γ-ray lines identified in overnight background spectra used to calibrate energy spectra[15].

E_{line} (keV)	Isotope
766.36	^{234m}Pa
1001.03	^{234m}Pa
1193.77	^{234m}Pa
1460.83	^{40}K
1737.73	^{234m}Pa
1911.17	^{234m}Pa
2204.21	^{214}Bi
2614.49	^{208}Tl

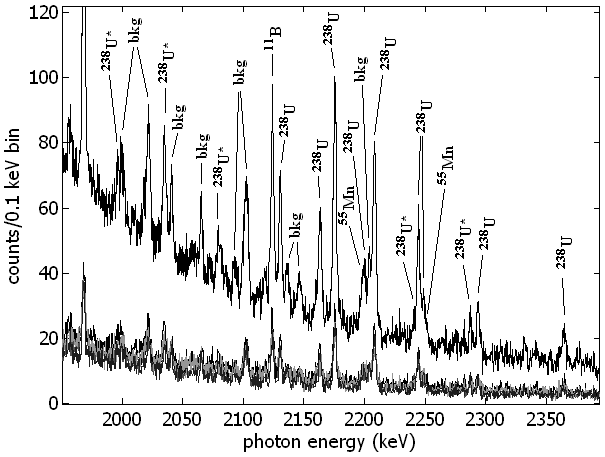

Figure 3: Spectra from all four detectors collected during run 1. The lower spectra are from the four different detectors before summing. Summing of these spectra produce the upper spectrum, which includes labeling to indicate the source of identified peaks. 'bkg' indicates the peak is present in the radioactive background spectrum, '^{238}U' indicates the peak is due to a known ^{238}U NRF resonance, and '^{238}U*' indicates the peak is suspected to be due to ^{238}U NRF.

To correct for varying beam intensity and the differing photon attenuation lengths of the targets, the rates at which 511-keV γ-rays were measured in the detectors were compared between runs. To consider the accuracy of this normalization and its potential contribution as a source of systematic errors, a series of calculations were performed using MCNPX. The calculations simulated a bremsstrahlung spectrum transported through the four different targets. The photon spectra that reached the transmission detection sheet after emission from each of the assay targets is defined as $\Phi^i(E)$, where the superscript indicates the target used in the run whose number is indicated in Table 2. Each of these computed spectra were also convolved with the cross section for pair production in U[16] to provide a quantity proportional to the rate at which pair pro-

duction occurred in the transmission detection sheet,

$$R^i_{\rm PP} = \int \Phi^i(E)\sigma_{\rm PP}(E)dE \quad (6)$$

The values of $R^1_{\rm PP}$ and $R^2_{\rm PP}$ differ by about 10%, whereas $R^3_{\rm PP}$ and $R^4_{\rm PP}$ differed from $R^1_{\rm PP}$ by about 3%. Computed photon spectra, $\Phi^i(E)$, were then normalized by dividing each spectrum by $R^i_{\rm PP}$, and compared. The quantity,

$$\Phi^i_N(E) = \frac{\Phi^i(E)/R^i_{\rm PP}}{\Phi^1(E)/R^1_{\rm PP}} \quad (7)$$

is shown in Figure 4 for the three targets containing DU. If the simulations indicated that normalization by measured pair production rates were perfect, the functions, $\Phi^i_N(E)$ would be unity at all energies. The calculations indicate that below approximately 1.8 MeV, normalizing spectra incident upon the transmission detection sheet by the intensity of pair production would result in large errors. However, the normalization needs only to be accurate in the range of the NRF resonances: 2.1-2.5 MeV. In this range the calculations indicate that by using the measured 511-keV peak to normalize the intensity of photons reaching the transmission detection sheet after penetrating through differing targets, should incur less than a 1.5% systematic error. The error bars in Figure 4 indicate the uncertainty of the MCNPX calculation, and do not include the systematic error due to the linear, rather than logarithmic, interpolation of atomic scattering functions that is performed in MCNPX[17]. The saw-tooth shape of the inset in Figure 4 can be attributed to these interpolation errors, and therefore the actual systematic error due to this normalization technique may be closer to 0.5%.

This normalization technique also automatically accounts for differing non-resonant attenuation of photons in the assay targets due to varying compositions, and systematic uncertainties that may arise due to errors in electron beam integration because neither of these quantities is directly used in the analysis. Instead, the intensity of the measured 511 keV photopeak provides a measured quantity that is linearly proportional to the intensity of 2-2.5 MeV photons that reach the transmission detection foil with the uncertainty discussed above. Given that statistical uncertainties described in Table 4 are between 6.7% and 28%, the addition of a systematic error of less than 1.5% will have little effect on the overall conclusions.

^{238}U NRF peaks identified in runs 2-4 were fit, integrated, and compared to corresponding peak intensities from run 1. The comparison of peak intensities is expressed as

$$\mathbb{A}^i_{E_{pk}} = \frac{A^i_{E_{pk}}}{A^1_{E_{pk}}}\frac{A^1_{511}}{A^i_{511}} \quad (8)$$

where $\mathbb{A}^i_{E_{pk}}$ is the relative intensity of the peak at $E = E_{pk}$ for run i, relative to run 1. $A^i_{E_{pk}}$ corresponds to the fit area of that peak. Each resonance yielded two observable peaks, due to de-excitation of the NRF level directly to the ground level, and also due to de-excitation via the first-excited state. The two

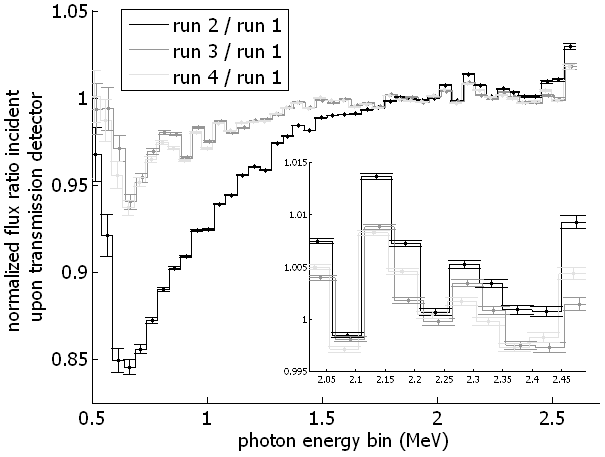

Figure 4: Calculated values of $\Phi^i_N(E)$, given by Equation 7 for the measurement of the targets containing DU, i=2,3 and 4.

values of $\mathbb{A}^i_{E_{pk}}$ for each level were combined via a weighted averaging, resulting in a single value of $\mathbb{A}^i_{level}$ for each NRF level, measured in each of runs 2-4. These values are shown with statistical uncertainties in the last columns of Table 4.

6. Areal Density Measurement

The areal density of an isotope in an irradiated target is related to the attenuation of resonant energy photons, as observed by a reduction in the relative rate that radiation detectors measure NRF γ-rays emitted from the transmission detection sheet. For each ^{238}U resonance, a function was derived (see the Appendix) that relates the rate at which NRF γ-rays are emitted from the transmission detection sheet to the areal density of ^{238}U in the assay target assuming that the effects of atomic absorption are similar between the different targets. This function, for a target containing the measured isotope at an atomic areal density, Nx, is given by

$$\mathbb{A}_{\rm model}(Nx) = C_{\rm notch}\frac{\int \lambda(t_{\rm TD},E)\exp[-\sigma_D(E)Nx]\sigma_D(E)dE}{\int \lambda(t_{\rm TD},E)\sigma_D(E)dE} \quad (9)$$

where $\lambda(t_{\rm TD},E)$ is the effective thickness a photon of energy, E, traverses in a transmission detection sheet having a thickness, $t_{\rm TD}$, and atom density, $N_{\rm TD}$, given by

$$\lambda(t_{\rm TD},E) = \frac{1-\exp[-(\alpha+N_{\rm TD}\sigma_D(E))t_{\rm TD}]}{\alpha+N_{\rm TD}\sigma_D(E)} \quad (10)$$

and $\alpha = \mu_{nr}[1+1/\cos(\theta)]$ and $\theta \approx 62^{\rm o}$ for the experimental geometry. The quantity, μ_{nr} contains the attenuation coefficients for all non-resonant photon scattering events in U, as retrieved from the XCOM database[16] and multiplied by the measured density of the DU in the transmission detection sheet.

The quantity, $C_{\rm notch}$, accounts for notch refill. To obtain values of $C_{\rm notch}$, simulations of the experimental geometry were conducted using MCNPX and the new NRF data library[18] to obtain $\mathbb{A}(\rho)$. These values were compared to analytical evaluations of $\mathbb{A}_{\rm model}/C_{\rm notch}$, giving $C_{\rm notch}$. Values of $C_{\rm notch}$ are shown

Table 4: Predicted and measured values of $\mathbb{A}^i_{level}$, the excess attenuation of resonant-energy photons compared to run 1. The levels at 2080 and 2287-keV have not been previously reported and therefore no prediction of $\mathbb{A}^i_{level}$ was made. Predicted values of $\mathbb{A}^i_{level}$ are obtained from evaluation of Equation 9 using the values of Γ and Γ_0 reported in Heil et al. and assuming that $C_{\text{notch}} = 1$. Column C uses values of Γ and Γ_0 from ENSDF and $C_{\text{notch}} = 1$. Columns B and D use the same resonance parameters as A and C, respectively, but use the best-estimate of C_{notch} such as those shown in Figure 5.

	E_{level}	predicted attenuation					measured	
	(keV)	A	B	C	D	uncertainty	attenuation	
run 2	2175.6	0.54	0.57	0.55	0.58	±0.018	0.58	±0.05
	2208.2	0.55	0.58	0.57	0.59	±0.019	0.62	±0.06
	2246.7	0.71	0.73	0.72	0.74	±0.016	0.72	±0.09
	2293.8	0.87	0.87	0.87	0.88	±0.014	0.94	±0.16
	2409.7	0.78	0.80	0.79	0.80	±0.013	0.84	±0.16
	2467.4	0.76	0.78	0.77	0.79	±0.016	0.65	±0.18
	2080.0						0.87	±0.15
	2287.4						0.67	±0.27
run 3	2175.6	0.88	0.89	0.88	0.89	±0.006	0.92	±0.06
	2208.2	0.88	0.89	0.89	0.90	±0.006	0.93	±0.07
	2246.7	0.93	0.94	0.94	0.94	±0.004	0.84	±0.09
	2293.8	0.97	0.97	0.97	0.97	±0.003	0.99	±0.16
	2409.7	0.95	0.95	0.95	0.96	±0.003	1.00	±0.16
	2467.4	0.95	0.95	0.95	0.95	±0.004	1.02	±0.21
	2080.0						0.99	±0.18
	2287.4						0.75	±0.27
run 4	2175.6	0.77	0.79	0.78	0.79	±0.011	0.82	±0.06
	2208.2	0.78	0.80	0.79	0.81	±0.011	0.80	±0.07
	2246.7	0.87	0.88	0.88	0.89	±0.008	0.89	±0.10
	2293.8	0.94	0.95	0.95	0.95	±0.006	0.84	±0.15
	2409.7	0.91	0.91	0.91	0.92	±0.006	1.00	±0.17
	2467.4	0.90	0.90	0.90	0.91	±0.007	1.04	±0.22
	2080.0						0.90	±0.16
	2287.4						0.59	±0.37
	χ^2	6.84	4.79	5.72	4.34			

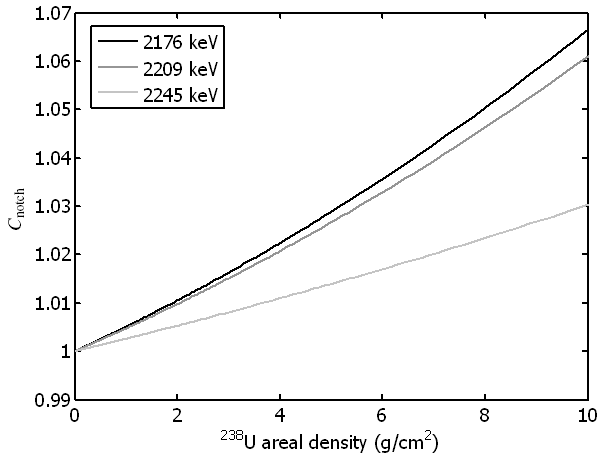

Figure 5: Estimated intensities of notch refilling for three ^{238}U resonances indicated by their centroid energy.

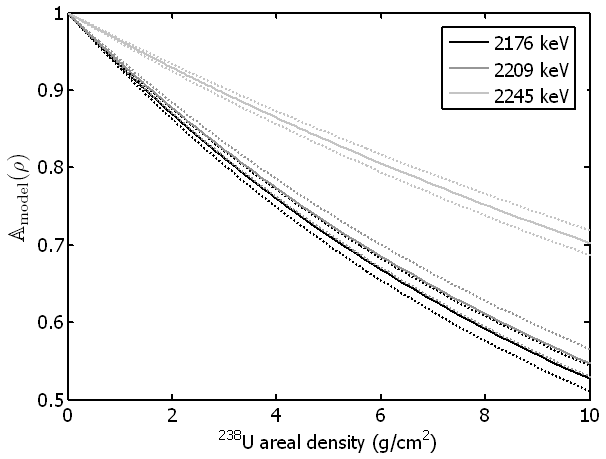

Figure 6: Predicted values of $\mathbb{A}_{\text{model}}(\rho)$ for three strongest ^{238}U resonances measured. Dotted lines indicate $\pm 1\sigma$ errors due to uncertainty in the strengths of the resonances from the Heil et. al. measurement.

in Figure 5 for the 2176, 2209 and 2245-keV ^{238}U resonances. The notch refill process is most intense for stronger and lower-energy resonances, and is more important for thicker targets. As seen in Figure 5, the effect of notch refill is estimated not to exceed 5% for this experiment.

Columns A-D in Table 4 present calculated values of $\mathbb{A}_{\text{model}}(\rho)$ for four different treatments of Equation 9. Values in columns A and B assume that the resonance parameters as reported by Heil are correct, whereas the values in columns C and D were obtained using the resonance parameters described in ENSDF. Columns A and C assume that $C_{\text{notch}} = 1$, and columns B and D use the estimates of C_{notch} such as those shown in Figure 5. The χ^2 values shown in the last row of Table 4 are determined by comparing the 18 measured $\mathbb{A}^i_{level}$ values to the predicted values shown in columns A-D. Only the statistical uncertainties of each measurement were used to calculate the reported χ^2 values[2]. Use of the notch-refill correction and the ENSDF evaluation of the resonance parameters (column D) provided the best agreement between data and prediction and therefore this treatment is used to determinate ^{238}U areal densities in the targets as measured by transmission NRF. The predicted attenuation values shown in column B, using the Heil interpretation of the resonance data with the notch refill correction, demonstrate better agreement to the data than either predicted attenuation that omitted the notch refill correction.

Using the values, $C_{\text{notch}}(\rho)$ shown in Figure 5 and the resonance parameters from ENSDF, Equation 9 is evaluated and values of $\mathbb{A}_{\text{model}}(\rho)$ corresponding to values in column D of Table 4 are shown in Figure 6. The dotted lines indicate errors due to the uncertainty of Γ_0 from the previous measurement of the ^{238}U resonances.

Each measured value of $\mathbb{A}^i_{level}$ shown in Table 4, $\mathbb{A}_{model}(\rho)$ was inverted to obtain an areal density of ^{238}U that would produce the corresponding attenuation. These values were combined for the six known resonances by calculating the weighted average of each estimated areal density. The weighted averages are shown in Table 5 with experimental statistical errors and systematic errors due to uncertainties in the strengths of the ^{238}U resonances. The agreement between areal density values that were obtained from the measured attenuation of resonant energy photons and from direct measurement of the targets indicates that this method can be used to non-destructively measure actinide concentrations at 1% levels in a matrix whose areal density is comparable to that of a spent fuel assembly.

Table 5: Values of the measured areal density of ^{238}U obtained by analysis of NRF peaks, and by direct measurement of the mass and area of the ^{238}U plates used in the assay target. The first errors listed for the NRF measurement are 1σ errors due to counting statistics in this experiment. The second stated errors are due to the uncertainties in values of Γ_0 extracted from Heil.

Run	NRF-measured ρx (g/cm^2)	direct ρx (g/cm^2)
2	$8.14 \pm {}^{0.98}_{0.99} \pm 0.49$	8.47 ± 0.08
3	$1.37 \pm 0.68 \pm 0.08$	1.69 ± 0.02
4	$3.12 \pm {}^{0.73}_{0.76} \pm 0.15$	3.34 ± 0.03

7. Resonance Parameters

This experiment not only demonstrates a transmission NRF measurement of ^{238}U and relates this to the ^{238}U areal density in thick targets, but is also an independent measurement of many ^{238}U resonance parameters. Comparing the measured intensities of γ-rays due to de-excitation to the ground state and first-excited states, the data provide $\Gamma_1 W_1(\theta)/\Gamma_0 W_0(\theta)$ for each resonance, shown in Table 6. These values were collected for each of the four runs, and remained constant within statistical uncertainties between runs, as expected.

Instead of using the Heil data to predict the resonant attenuation of photons incident upon the targets, the known areal densities of the targets and the attenuation of resonant-energy photons can be used to estimate Γ_0 for each resonance. These

[2]Inclusion of the statistical uncertainties reported by Heil into the χ^2 calculation does not significantly alter the results.

values, the corresponding values extracted from Heil, and the recommended values, obtained by a weighted average of the two, are shown in Table 6. The inverse of the variance of each Γ_0 was used as the weight for averaging. The transmission measurement indicates that the values of Γ_0 for the two largest resonances may be lower than reported by Heil, whereas for the 2245-keV resonance, Γ_0 may be slightly larger or possibly $\Gamma > \Gamma_0 + \Gamma_1$ for this state. Limited counting statistics prohibit stronger statements regarding the possibilities of systematic disagreements between these data and those obtained by Heil et al.

Six additional γ-rays were identified in the beam-on spectrum that were neither present in the radioactive background, nor previously published[3]. Their energies were 1996.6 ± 0.3, 2035.0 ± 0.2, 2080.0 ± 0.2, 2146.0 ± 0.3, 2241.1 ± 1.0, and 2287.4 ± 0.6 keV. Besides the 2241 and 2287 keV lines, each line was well-isolated and at least 5 standard deviations above the randomly varying background. The 2287 peak was also significantly stronger than background but was not well-resolved in energy from the known 2294 keV NRF γ-ray[4]. The 2241 keV peak was a minor contributor to a multiplet dominated by the known 2245 keV ^{238}U NRF γ-ray. The 2241 keV peak was identified by its influence on the multiplet shape, however its energy and intensity were significantly less well-determined than the other peaks.

The pairs of γ-rays at 2035.0 and 2080.0 keV, and at 2287.4 and 2241.1 keV could indicate the pattern of de-excitation of one excited nuclear state via γ-ray emission populating the ground state or the first excited state. Using the transmission measurement to estimate Γ_0 for the 2080 and 2287-keV resonances resulted in very large uncertainties (shown in Table 6). Values of Γ_0 may also be estimated by comparing the γ-ray intensities to those observed for a larger state, such as the 2176-keV resonance. Correcting for the differences in bremsstrahlung intensity, resonant and non-resonant attenuation of photons in the assay targets, and full γ-ray detection efficiencies of the HPGe detectors, the strengths of the 2080 and 2287-keV resonances are 0.38 ± 0.03, and 0.12 ± 0.06, respectively, relative to the 2176-keV resonance. If both states are spin-1, their ground-state widths would be the values shown in the fifth column of Table 6, whereas if the spin of the excited state were $2\hbar$ (J=2), the values of Γ_0 would be reduced by 3/5.

Two additional γ-ray lines were detected at 1996.6 ±1 and 2146.0 ±0.3 keV. Their intensities are 0.18 ±0.05 and 0.15 ±0.05, respectively, relative to the 2176-keV line. The energies of these γ-rays differ by 149.4 ±0.7 keV, which could indicate that they are both due to de-excitation of an additional 2146-keV NRF state. If this were true, the 1996.6-keV γ-rays would be due to de-excitation via photon emission to the second-excited, 148.4-keV ^{238}U level with spin-4^+. An additional γ-ray would be expected at 2101.1 keV, corresponding to de-excitation of the resonance to the first-excited state. The presence of this γ-ray in the spectra could not be confirmed due to a relatively strong background line at 2103-keV attributed to the ^{208}Tl single-escape peak.

[3]Two additional ^{238}U NRF states at 2090 and 2145 keV have included in Figure 3 of Reference[19], but no discussion of the states has been published, nor are they present in the ENSDF.

[4]Reported by Heil et al. to be 2295 keV.

8. Discussion

Performing a transmission measurement to relate the areal density of ^{238}U in the target to the excess attenuation of resonant photons warrants explicit consideration of the sources of errors that enter into the measurement. The foremost source of error is that due to counting statistics. The largest NRF γ-ray lines resulted in approximately 2500 full-energy events measured by the germanium detectors during a measurement, indicating the smallest statistical error allowed by the data is 2%. However, since the measurements are relative, the statistical errors must be propagated through Equation 8, resulting in the statistical errors presented in the last column of Table 4.

Making relative measurements in a geometry in which the transmission detection sheet has a fixed position reduces the potential for systematic uncertainties. The assay targets, positioned upstream, are sufficiently large that they subtend the entire profile of the bremsstrahlung beam leaving the collimator, thereby rendering their positioning insensitive to total results. However, the sheets comprising the DU in the assay targets could have been positioned such that they were not perfectly normal to the beam trajectory which would effectively increase the ^{238}U areal density through which the bremsstrahlung photons would penetrate. Although difficult to quantify, care was taken to visually inspect the alignment of the DU sheets, and due to the area size of the DU plates (20 cm on a side), small deviations in alignment are easy to observe. A placement of the plates 5^o from beam normal would result in the DU plate's corners being 1.8 cm from square, which is easily observable. Conversely, a 5^o rotation of a DU sheet only increases the areal density through which photons penetrate by 0.38%, which is small compared to other errors. We therefore conclude that target positioning is not an important contributor to the error in the measurement.

Relating the measured reduction in NRF count rates to areal density incurs additional systemic errors due to the uncertainty with which the ^{238}U NRF parameters are known. The reported uncertainties in the resonance parameters have been propagated through the process of inverting Equation 9, predicting how the ^{238}U areal density determinations would change if the intensity of each resonance were altered by $\pm 1\sigma$. These calculations produced the systematic uncertainty errors reported in Table 5.

The most complex portion of the analysis and potentially an important source of systematic error is the use of the 511 keV normalization routine described in Section 5. Comparing spectra obtained while the transmission detection sheet is present in the beam to those obtained when the sheet is absent from the beam indicate that the vast majority of measured 511 keV photons are due to the presence of the transmission detection sheet in the beam. Likewise, using MCNPX to estimate the size of the error induced by this normalization routine indicated that the rate at which 511 keV photons were produced in the transmission detection sheet was very nearly linearly proportional to the flux of photons with energies between 2 and 2.5 MeV

Table 6: First column: centroid energies of ^{238}U levels observed to undergo NRF. Second column: measured relative intensities of γ-rays due to de-excitation of NRF levels to the first-excited and ground states. Third column: values of Γ_0 that best represent the measured attenuation of resonant-energy photons. Fourth column: values of Γ_0 taken from Heil, if it is assumed that $\Gamma = \Gamma_0 + \Gamma_1$. Fifth column: the Γ_0 values, obtained for known resonances by weighted averaging of the values in columns 3 and 4. *The values of Γ_0 for the 2080 and 2287-keV states were obtained by comparing γ-ray intensities to those emitted from the 2176-keV resonance. These values assume the resonant state is spin-1 and would be smaller by 3/5 if the excited state were spin-2.

E_{level}	this experiment				Heil et al.		best-estimate	
(keV)	$\Gamma_1 W_1/\Gamma_0 W_0$		Γ_0 (meV)					
2176	0.55	± 0.06	30.59	±4.50	36.02	±2.18	34.99	±1.96
2209	0.53	± 0.07	30.83	±5.71	35.03	±2.27	34.46	±2.11
2245	0.52	± 0.09	23.14	±7.48	19.70	±1.38	19.81	±1.36
2295	0.92	± 0.23	7.14	±11.00	8.43	±0.96	8.42	±0.96
2410	0.60	± 0.16	10.56	±13.98	16.94	±1.21	16.89	±1.21
2468	0.72	± 0.26	24.25	±22.67	20.10	±1.64	20.12	±1.64
2080	2.39	± 0.63	4.97	±5.25	x		12.9*	± 1.0
2287	0.41	± 0.32	37.60	±30.37	x		5.1*	± 2.6

that reached the transmission detection sheet, regardless which of the four targets was measured. The deviation from linearity was largest when the flux due to the target in run 1 was compared to that in run 2, and resulted in up to a 1.5% difference (see Figure 4). This is significantly smaller than the error due to counting statistics, and is likewise significantly smaller than the statistical errors that would result if the measured NRF γ-rays due to ^{11}B were instead used to normalize the spectrum. It should be emphasized that MCNPX was only used to estimate the precision of the 511 keV normalization routine, and no effort was made to use the results of MCPNX to correct for the potential systematic error resulting from the routine.

Conversely, MCNPX was used to predict and correct for notch refill. This could in principle lead to further systematic uncertainties. However, C_{notch} in Equation 9 took values between 1.00 and 1.05, therefore even 100% uncertainties in the notch refill correction would result in no more than a 5% change in the predicted values of $\mathbb{A}_{\text{model}}$ and this would likewise only change ^{238}U areal densities predicted by this method by an amount similar to the systematic error values shown in Table 5. It is not expected that the notch refill estimate would be this imprecise, and it is worth noting that the corrections produced by comparing MCNPX calculations to the analytical model that explicitly neglects down-scattered resulted in resonant attenuation predictions that better agreed with the experimental data. Furthermore, comparing the experimentally measured attenuation values with the predicted values indicate that larger values of C_{notch} would produce better agreement.

To summarize, the largest source of experimental errors is the uncertainties relating to counting statistics. All systematic sources of error are expected to result in uncertainties that are less than these statistical errors. The uncertainty due to the resonance parameters reported by Heil provide the largest source of systematic error and are included in Table 5. The MCNPX-predicted correction of the analytical model due to the notch refill process results in better agreement between ^{238}U areal densities derived from NRF transmission measurements and those from direct measurement of target masses. The systematic uncertainty of this correction, even if a large fraction of the total correction does not significantly modify the experimental results. Finally, because of target and transmission foil constraints and the relative nature of the measurements, we assert that any systematic errors due to imprecisely known geometry would be negligible.

9. Conclusion

The determination of ^{238}U areal densities ranging between 1.7 and 8.5 g/cm^2 in an approximately 86 g/cm^2 target by observation of attenuation of resonant-energy photons has been accomplished. While previous transmission measurements using quasi-monoenergetic photon sources have indicated null results for the observation of notch refill[4], the data obtained in this experiment, using thick targets and a bremsstrahlung beam have exhibited a trend indicative of notch refill that could increase the measured NRF rate by up to 5% for large resonances and the target containing the most ^{238}U. The geometric arrangement wherein DU preceded Pb in the target represents the most probable geometry in which to observe notch refill. A correction based on the MCNPX modeling has been implemented in the analysis producing the areal densities measured by transmission NRF. Without the notch refill correction, the data tend to under-predict the areal density of ^{238}U in the target by approximately twice the standard deviation estimated by Poisson counting statistics.

This experiment indicated that the ^{238}U resonance parameters reported by Heil resulted in under-predicted ^{238}U areal densities, primarily due to the 2176 and 2209-keV resonances. Inclusion of a notch refill correction that was based on comparing MCNPX results with an analytical model that excluded photon down-scatter improved the agreement between the predicted and experimentally observed attenuation. This agreement would also be improved if the actual correction due to notch refill correction were slightly larger than indicated by our modeling.

To within statistical uncertainties, the measurement agrees with models used to describe resonant attenuation and subsequent measurement of fluorescence emitted from the transmission detector. However, it also indicates the difficulty of using transmission nuclear resonance fluorescence to precisely measure small quantities of an isotope in an assay target. Rates at which statistics accrue in a transmission measurement are

strongly dependent on the strengths of the resonances used for the measurement. Measurements of NRF in ^{235}U and ^{239}Pu have indicated their resonances are smaller than those examined here. This indicates that a transmission NRF measurement that is useful for nuclear safeguards applications would require a significantly more intense photon source than the 65 μA bremsstrahlung beam used in this experiment. Higher current electron accelerators are commercially available[20]. However, required photon count rates pose difficult challenges for semiconductor detectors and energy resolution requirements make scintillating detectors less attractive. These constraints are the subject of further study.

The extended measurement of ^{238}U NRF has also led to observation of two new excited states and a potential third state. The state at 2080 keV is fairly strong, but appears to preferentially decay by emission of 2035-keV γ-rays, producing the first-excited state of ^{238}U. This raises the question as to whether the angular momentum of the state is $2\hbar$ ($J = 2$), or whether the projection of the angular momentum of the state onto the nuclear symmetry axis is zero ($K = 0$). The latter type of state is predicted by the Alaga sum rules to decay with $\Gamma_1/\Gamma_0 = 2$[1]. The 2287-keV state is quite weak but demonstrates the more typical de-excitation pattern of preferential decay by emission of a single γ-ray to populate the ground state. The γ-rays emitted from this state appears slightly above the considerable photon background and would be difficult to observe using higher endpoint-energy bremsstrahlung beams because such beams reduce the signal intensity, relative to background. Finally, γ-rays with energies of 1996 and 2146 keV could indicate a 2146-keV resonant state, although the presence of the broad ^{208}Tl escape peak obstructs confident observation of a 2101-keV γ-ray that would strongly support this hypothesis.

Acknowledgements

The authors would like to thank Chatham Cooke for his operation of the Van de Graaff accelerator at the High Voltage Research Laboratory (HVRL) at MIT.

This work is supported by the Office of Proliferation Detection (US DOE, NA-221), the MPACT campaign of FCR&D program of the Office of Nuclear Energy (US DOE), and the Director, Office of Science of the US Department of Energy at the Lawrence Berkeley National Laboratory under contract number DE-AC02-05CHI1231.

Appendix A. Derivation of Relationship between Areal Density and Relative Rate of Measured NRF γ-rays

The rate at which NRF signals due to photons of energy, E, are detected by a radiation detector from a location, $\mathbf{r}$, within the target volume, V, is given by:

$$\frac{d^2R_{\mathrm{NRF}}}{dVdE} = N\Phi(E,\mathbf{r})\sigma_{\mathrm{NRF}}(E)W_e(\theta)\exp[-\mu(E_\gamma)r_o] \times\left[\epsilon(E_\gamma)\frac{\Omega(\mathbf{r})}{4\pi}P_f(E_\gamma)\right] \quad (A.1)$$

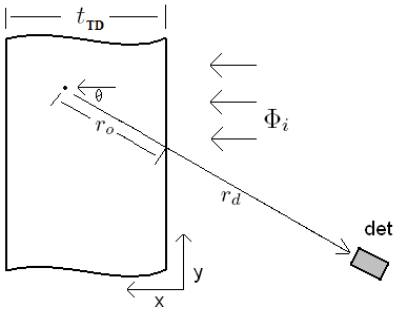

Figure A.7: Schematic drawing of slab geometry assumed for NRF count rate derivation.

Where N is the number density of atoms in the target that undergo NRF with cross section $\sigma_{\mathrm{NRF}}(E)$, $\Phi(E,\mathbf{r})$ is the energy-differentiated photon flux at the point $\mathbf{r}$, $W_e(\theta)$ is the effective angular correlation function taking into account the finite solid angle of the detector, r_o is the distance traversed by the NRF γ-rays as it leaves the target in the direction of a detector, E_γ is the energy of the emitted NRF γ-ray, which interacts within the target material with probabilities described by an attenuation coefficient, $\mu(E_\gamma)$ that results in a total attenuation of NRF γ-rays leaving the target of $\exp[-\mu(E_\gamma)r_o]$, $\epsilon(E_\gamma)$ is the probability that the radiation detector measures the full energy of an incident NRF γ-ray, $\frac{\Omega(\mathbf{r})}{4\pi}$ is the fraction of the solid angle subtended by the radiation detector from the point where the γ-ray is emitted, and $P_f(E_\gamma)$ is the probability that the NRF γ-ray penetrates through the radiation filter without interacting. γ-rays emitted after NRF are reduced in energy due to the energy taken by the recoiling nucleus. This energy reduction is sufficient for interactions considered here to assume that the interaction cross section for NRF γ-rays is only due to nonresonant interactions.

Appendix A.1. NRF Rates for Photons Incident Upon a Uniform Slab

The transmission detection sheet may be considered a slab of thickness, t_{TD}, that is irradiated with a uniform parallel beam of intensity, Φ_i, that is normally incident upon the slab. A radiation detector is assumed to be located sufficiently far from the target that the beam diameter and t_{TD} are negligibly small compared to the detector distance, r_d. A schematic rendering of this geometry is shown in Figure A.7. Although not indicated, the experimental geometry may also include a filter in front of the detector to reduce low-energy photon count rates.

For simplicity, we assume that we may neglect photon downscatter, then $\Phi(E,\mathbf{r})$ only varies due to the attenuation of photons:

$$\Phi(E,x) = \Phi_i(E)\exp[-\mu(E)x] \quad (A.2)$$

and $\mu(E)$ now contains both resonant and non-resonant contributions:

$$\mu(E) = \mu_{atom} + N_{\mathrm{TD}}\sigma_{\mathrm{D}}(E) \quad (A.3)$$

Considering only photon energies near an NRF resonance, we may neglect the energy-dependence of the non-resonant attenuation coefficient, μ_{atom}. Likewise, the attenuation coefficient for

NRF γ-rays, $\mu(E_\gamma) = \mu_{atom}$, because nuclear recoil has made them non-resonant, but has not altered their energies sufficiently to make the energy dependence of μ_{atom} relevant.

The length the photon must traverse to leave the target is given by $r_o = x/cos(\theta)$, where θ is the angle between the initial trajectory of an incident photon and the ray between the photon interaction point and the position of the radiation detector.

Substituting, the rate of detection of full-energy NRF γ-rays can be written as:

$$\frac{d^2R_{\rm NRF}}{dxdE} \approx \exp[-(\mu_{atom}[1 + 1/cos(\theta)] + N_{\rm TD}\sigma_{\rm D}(E))x] \times N_{\rm TD}\Phi_i(E)\sigma_{\rm D}(E)W_e(\theta)\frac{\epsilon A P_f(E_\gamma)}{4\pi r_d^2} \quad \text{(A.4)}$$

We define

$$\alpha = \mu_{atom}[1 + 1/\cos(\theta)] \quad \text{(A.5)}$$

and $\mu_{\rm NRF}(E) = N_{\rm TD}\sigma_{\rm D}(E)$ and obtain:

$$\begin{aligned}\frac{dR_{\rm NRF}}{dE} &= \int_0^{t_{\rm TD}} \frac{d^2R_{\rm NRF}}{dxdE}dx \\ &\approx \frac{1 - \exp[-(\alpha + \mu_{\rm NRF}(E))t_{\rm TD}]}{\alpha + \mu_{\rm NRF}(E)} \\ &\quad \times N_{\rm TD}\Phi_i(E)\sigma_{\rm D}(E)W_e(\theta)\frac{\epsilon A P_f(E_\gamma)}{4\pi r_d^2} \end{aligned} \quad \text{(A.6)}$$

Appendix A.2. Relative Rate of NRF γ-ray Detection in Transmission Measurement

Neglecting the down-scatter of photons, the effective photon flux leaving the target in a transmission measurement is given by,

$$\Phi_o(E) \approx \Phi_{beam}\exp[-N\sigma_{\rm D}(E)x]\exp\left[-\mu_{\rm atom}x\right] \quad \text{(A.7)}$$

where N is the atom density of the isotope being studied in the transmission measurement and x is the target thickness.

The photon flux due to photons that were not attenuated in the assay target, Φ_o is incident upon the transmission detection sheet, i.e. $\Phi_i = \Phi_o$, and therefore this flux is substituted into Equation A.6 yielding:

$$\begin{aligned}\frac{dR_{\rm NRF}}{dE} =& \lambda(t_{\rm TD}, E)\Big[\exp[-N\sigma_{\rm D}(E)x]\sigma_{\rm D}(E)\Big] \\ &\times \left[N_{\rm TD}\Phi_{beam}\exp(-\mu_{atom}x)W_e(\theta)\frac{\epsilon A P_f(E_\gamma)}{4\pi r_d^2}\right] \end{aligned} \quad \text{(A.8)}$$

The first term,

$$\lambda(t_{\rm TD}, E) = \frac{1 - \exp[-(\alpha + \mu_{\rm NRF}(E))t_{\rm TD}]}{\alpha + \mu_{\rm NRF}(E)} \quad \text{(A.9)}$$

is identical to Equation 10 and is an effective thickness that a photon experiences as it traverses the transmission detection sheet. The second term in Equation A.8 represents combination of the resonant attenuation of photons in the assay target and the NRF response of the transmission detection sheet. When comparing two transmission measurements with identical measurement geometries except slight variations in the composition of the assay target, we assume that the third term in Equation A.8 may be assumed to not significantly change between measurements.[5]

The energy resolution of high-purity germanium detectors is much wider than the widths of NRF resonances considered. Therefore energy-dependent variation in the first two terms in Equation A.8 will not be directly observed in the detected photon energy spectrum and instead, values of Equation A.8 that are integrated over an energy range given by the resolution of the detector will be measured. Since this range is significantly wider than the resonance, we assume that comparing the rate of measurement of a given NRF resonance may be accomplished by:

$$\mathbb{A}(Nx) = \frac{\int \lambda(t_{\rm TD}, E)\exp[-\sigma_{\rm D}(E)Nx]\sigma_{\rm D}(E)dE}{\int \lambda(t_{\rm TD}, E)\sigma_{\rm D}(E)dE} \quad \text{(A.10)}$$

To obtain Equation 9, Equation A.10 is further modified by addition of a multiplicative factor, $C_{\rm notch}$, which accounts for the fact that Equation A.2 is not exact and photons with energy, $E_{ph} > E$ may be down-scattered with the assay target to the considered energy, E.

References

[1] U. Kneissl, H.H. Pitz, and A. Zilges, Investigation of Nuclear Structure by Resonance Fluoresence Scattering, Prog. Part. Nucl. Phys. 37 (1996) 349-433.

[2] O. Beck, T. Ruf, Y. Finkelstein, M. Cardona, T.R. Anthony, D. Belic, T. Eckert, D. Jager, U. Kneissl, H. Maser, R. Moreh, A. Nord, H.H. Pitz, and A. Wolpert, Nondestructive determination of the ^{13}C content in isotopic diamond by nuclear resonance fluorescence, J. App. Phys. 83 (1998) 5484.

[3] W. Bertozzi, R.J. Ledoux, Nuclear resonance fluorescence imaging in non-intrusive cargo inspection, Nucl. Inst. Meth. B 241 (2005) 820-825.

[4] C.A. Hagmann, J.M. Hall, M.S. Johnson, D.P. McNabb, J.H. Kelley, C. Huibregtse, E. Kwan, G. Rusev, and A.P. Tonchev, Transmission-based detection of nuclides with nuclear resonance fluorescence using a quasi-monoenergetic photon source, J. App. Phys. 106, (2009) 084901.

[5] W. Bertozzi, J.A. Caggiano, W.K. Hensley, M.S. Johnson, S.E. Korbly, R.J. Ledoux, D.P. McNabb, E.B. Norman, W.H. Park, and G.A. Warren, Nuclear resonance fluorescence excitations near 2 MeV in ^{235}U and ^{239}Pu, Phys. Rev. C 78, (2008) 041601(R).

[6] H. Yang, D. Wehe, Detection of Concealed Special Nuclear Material Using Nuclear Resonance Fluorescence Technique, 2009 IEEE Nucl. Sci. Symp. Conf. Rec. N13-222 (2009).

[7] B.J. Quiter, B.A. Ludewigt, V.V. Mozin, and S.J. Tobin, Nondestructive Spent Fuel Assay Using Nuclear Resonance Fluorescence, Proc. INMM Conf., July 12-16, 2009, Tucson, AZ.

[8] B.A. Ludewigt, V.V. Mozin, A.R. Haefner, and B.J. Quiter, Using Nuclear Resonance Fluorescence for Nondestructive Isotopic Analysis, Proc. INMM Conf., July 11-15, 2010, Baltimore, MD.

[9] F.R. Metzger, Resonance Fluorescence in Nuclei, Prog. in Nucl. Phys. 7, (1959) 54.

[5] In the experiment described in this paper, the variation in assay targets, described in Table 2 indicate that this assumption could lead 20% errors. However, the 511 keV normalization routine accounts for differences in attenuation of photons with $E > 1.02$ MeV in the different assay targets.

[10] R. Vodhanel, M.K. Brussel, R. Moreh, W.C. Sellyey, and T.E. Chapuran, Strong *M1* transitions in ^{23}Na below 10 MeV, Phys. Rev. C 29 2 (1984) 409.
[11] R.D. Heil, H.H. Pitz, U.E.P Berg, U. Kneissl, K.D. Hummel, G. Kilgus, D. Bohle, A. Richter, C. Wesselborg, and P. Von Brentano, Observation of orbital magnetic dipole strength in the actinide nuclei ^{232}Th and ^{238}U, Nucl. Phys. A 476 (1988) 39-47.
[12] F.E Chukreev, V.E. Makarenko, M.J. Martin, Nucl. Data Sheets 97, (2002) 129 doi:10.1006/ndsh.2002.0017.
[13] J.F. Pelowitz (ed.), MCNPX^{TM} USERS MANUAL Version 2.6.0, LA-CP-07-1473 (2008).
[14] D.E. Cullen, J.H. Hubbell, L. Kissel, EPDL97: the Evaluated Photon Data Library, '97 Version. UCRL-504000 Vol 6, Rev. 5 (1997).
[15] L.P. Ekstrom and R.B. Firestone, WWW Table of Radioactive Isotopes, database version 2/28/99 from URL http://ie.lbl.gov/toi/index.htm
[16] M.J. Berger, J.H. Hubbell, S.M. Seltzer, J. Chang, J.S. Coursey, R. Sukumar, and D.S. Zucker, XCOM: Photon Cross Sections Database, NIST Standard Reference Database 8 (XGAM) available online at http://physics.nist.gov/PhysRefData/Xcom/Text/XCOM.html (1998).
[17] J.S. Hendricks and B.J. Quiter, MCNP/X Form Factor Upgrade for Improved Photon Transport, (LA-UR-10-01096) J. of Nuc. Tech. (2010). In Press.
[18] G.W. McKinney, A.B. McKinney, J.S. Hendricks, D.B. Pelowitz, B.J. Quiter, MCNPX NRF Library - Release 2, Proc. ANS Ann. Mtg. (San Diego, CA July 13-17, 2010).
[19] U. Kneissl, Photoexcitation of Low-Lying, Isovector 1^+ States in Deformed Nuclei, Prog. Part. Nucl. Phys. 24, 41 (1990).
[20] J. Pottier, A new type of RF electron accelerator: the rhodotron, Nucl. Instr. Meth. B40/41 (1989) 943-945.